label1]Mario Vazquez Corte [label1]Department of Computer Science. label2]Luis
V. Montiel [label2]Department of Operations Research and Industrial Engineering.
Instituto Tecnológico Autónomo de México - ITAM
Río Hondo 1, CDMX, México.

Abstract

We propose and analyze a new Markov Chain Monte Carlo algorithm that
generates a uniform sample over full and non-full dimensional polytopes. This al-
gorithm, termed "Matrix Hit and Run" (MHAR), is a modification of the Hit and
Run framework. For the regime $n^{1+\frac{1}{3}} \ll m$, MHAR has a lower asymptotic cost
per sample in terms of soft-O notation ($\mathcal{O}^*$) than do existing sampling algorithms
after a *warm start*. MHAR is designed to take advantage of matrix multiplication
routines that require less computational and memory resources. Our tests show
this implementation to be substantially faster than the *hitandrun* R package, es-
pecially for higher dimensions. Finally, we provide a python library based on
Pytorch and a Colab notebook with the implementation ready for deployment in
architectures with GPU or just CPU.

Sampling Polytopes Graphics Processing Unit Hit and Run Random Walk MCMC.

1   Introduction

Random sampling of convex bodies is employed in disciplines such as operations re-

search, statistics, probability, and physics. Among random-sampling approaches, Markov

Chain Monte Carlo (MCMC) is the fastest, most accurate, and easiest to use [Chen et al.(2018)Chen, Dw

MCMC is often implemented using polytope sampling algorithms, which are used in vol-

ume estimation [Lawrence(1991)] [Lee and Vempala(2018)] [Emiris and Fisikopoulos(2014)],

convex optimization [Vempala and Bertsimas(2004)] [Ma et al.(2019)Ma, Chen, Jin, Flammarion, and J

contingency tables [Kannan and Narayanan(2013)], mixed integer programming [Huang and Mehrotra(2

linear programming [Feldman et al.(2005)Feldman, Wainwright, and Karger], hard-disk

modeling [Kapfer and Krauth(2013)], and decision analysis [Tervonen et al.(2013)Tervonen, Valkenhoef,

[Montiel and Bickel(2013a)] [Montiel and Bickel(2013b)].

Sampling methods start by defining a Markov chain whose stationary distribution converges to a desired target distribution. Then they draw a predetermined number of samples. These methods have two sources of computational complexity: *mixing-time*, which is the number of samples needed to lose the "dependency" between each draw; and *cost per iteration*, which is the number of operations required to obtain a single sample. Sampling algorithms aim for efficient mixing-times, so that they can produce independent samples without dropping (also called "burning") too many of them, and a low cost per iteration in order to draw samples fast [Geyer and Charles(1992)].

1.1   History and relevance of MCMC

The use of Monte Carlo methods has surged in the last 50 years, due to the availability of modern computers. However, there are records of experiments leading to a Monte Carlo simulation method as early as 1901 when Mario Lazzarini approximate π by manually repeating Buffon's needle experiment 3,408 times. During the first half of the 20th century the use of Monte Carlo had a frequentist approach, since the Bayesian approach was viewed as unfavorable due to philosophical and computational considerations. With the advent of MCMC together with more powerful computers, Bayesian Monte Carlo methods saw an increase in use, having its first application published in 1993 with the "the bootstrap filter" [Gordon et al.(1993)Gordon, Salmond, and M.].

Recently, numerous applications in operations research have used MCMC to complement diverse optimization models. For example, the characterization of a joint probability distribution under partial information is perhaps not unique [Montiel and Bickel(2013b)]. Hence, if we need the joint probabilities to value a real option [Montiel and Bickel(2012)], or to optimize the net gain of an oil field [Montiel and Bickel(2013a)], we have to understand the space to which the joint distribution belongs. Another example is the incomplete specification of a multi-attribute utility function in decision analysis. Here, the problem is to understand the range of preferences of the decision maker to provide recommendations [Tervonen et al.(2013)Tervonen, Valkenhoef, Basturk, and Postmus], [Montiel and Bickel

2

In cooperative game theory [Cid and Montiel(2019)], MCMC can be used to create an approximate objective function to optimize the negotiation strategy for a coalition of players.

1.2 The blueprint

This work presents an algorithm we call Matrix Hit and Run (MHAR) for sampling full and non-full dimensional polytopes. MHAR enhances the Hit-and-Run (HAR) algorithm proposed in [Montiel and Bickel(2013a)]. We use the standard definition of a generic polytope $\Delta := \{x \in \mathbb{R}^n | Ax \leq b\}$, where $(A, b) \in \mathbb{R}^{m \times n} \times \mathbb{R}^{m \times 1}$, n is the number of elements of x, $m = m_E + m_I$ is the number of restrictions, m_E is the number of equality constraints, and m_I is the number of inequality constraints.

The contribution of this work is six-fold:

- First, we introduce Matrix Hit-and-Run (**MHAR**).

- Second, we show that the cost per sample of the MHAR depends entirely on m, n, z, and ω, where m, n are as described in the definition of Δ, ω represents a matrix multiplication coefficient as described in Table 1, and z is a padding hyper-parameter specified by the user. After proper pre-processing and a warm start, the algorithm has a cost per sample of $\mathcal{O}^*\big(\min(m_I^{\omega-2}n^4, m_I n^{\omega+1})\big)$ for the full dimensional scenario, and of $\mathcal{O}^*\big(\min(n^{\omega+2}, m_I n^{\omega+1})\big)$ for the non-full dimensional one.

- Third, we demonstrate that MHAR has lower cost per sample than HAR if the hyper-parameter z is bigger than $\max(n, m)$. This is achieved by switching possibly isolated *walks* into a padded matrix that allows us to share operations between walks.

- Fourth, we show that after proper pre-processing and a warm start, MHAR has a lower asymptotic cost per sample for the regime $n^{1+\frac{1}{3}} \ll m$ than does any of the published sampling algorithms [Chen et al.(2018)Chen, Dwivedi, Wainwright, and Yu].

3

- Fifth, we provide code for MHAR as a python library based on the Pytorch framework. It is ready for use in CPU or CPU-GPU architectures (as found in Colab, AWS, Azure, and Google Cloud). All MHAR experiments were conducted using Colab notebooks with an Nvidia P100 GPU. The code is available in `https://github.com/uumami/mhar_pytorch`.

- Sixth, we present the results of experiments to assess the performance of MHAR against the *hitandrun* package used in [Tervonen et al.(2013)Tervonen, Valkenhoef, Basturk, and P MHAR was found to be substantially faster in almost all scenarios, especially in high dimensions. Furthermore, we ran simulations to empirically test the convergence in distribution of our implementation, with favorable results. Finally we present insights over the padding hyper-parameter z obtained via computational tests.

The remainder of this paper is organized as follows. §2 revises definitions and some basic matrix-to-matrix operations. §3 revisits the cost per iteration and cost per sample of HAR. §4 provides a computational complexity analysis of MHAR. §5 compares MHAR against other algorithms developed for full dimensional scenarios. §6 contains a back-to-back comparison of our implementation against the *"hitandrun"* library used in [Tervonen et al.(2013)Tervonen, Valkenhoef, Basturk, and Postmus], and a numerical analysis of the padding parameter z. §7 presents our conclusions and identifies future work.

For clarity and simplicity, HAR will refer to the algorithm presented in [Montiel and Bickel(2013a)], which extends [Smith(1996)] for non-full dimensional polytopes. For ease of comparison, we use "soft-O" notation $\mathcal{O}^*$, which suppresses $log(n)$ factors and other parameters like error bounds [Chen et al.(2018)Chen, Dwivedi, Wainwright, and Yu], [Lee and Vempala(2018)], [Lovász(1999)]. In order to allow comparison with other algorithms, we assume that the polytope sampled by HAR and MHAR has received proper pre-processing, which means the polytope is in near isotropic position as defined in [Chen et al.(2018)Chen, Dwivedi, Wainwright, and [Lee and Vempala(2018)], [Tervonen et al.(2013)Tervonen, Valkenhoef, Basturk, and Postmus].

Additionally all algorithms are compared from a *warm start*. We use $f \ll g$ notation to define a relation where $f \in \mathcal{O}(g)$. Finally, we assume the existence of a random stream of bits that allow us to generate a random number in $\mathcal{O}(1)$.

2 Preliminaries

This section formalizes the notation and provides a brief overview of computational complexity in matrix-to-matrix operations.

2.1 Polytopes

We start by defining a polytope, which is the n-dimensional generalization of a polyhedron, as the intersection of half-spaces. Formally, a polytope is characterized by a set of m_E linear equality constraints and m_I linear inequality constraints in a Euclidean space ($\mathbb{R}^n$):

$$\Delta^I = \{x \in \mathbb{R}^n \mid A^I x \leq b^I,\ A^I \in \mathbb{R}^{m_I \times n},\ b^I \in \mathbb{R}^{m_I}\}, \tag{1}$$

$$\Delta^E = \{x \in \mathbb{R}^n \mid A^E x = b^E,\ A^E \in \mathbb{R}^{m_E \times n},\ b^E \in \mathbb{R}^{m_E}\}, \tag{2}$$

$$\Delta = \Delta^I \cap \Delta^D, \tag{3}$$

where Equations (1) and (2) are defined by the inequalities and equalities, respectively. The third equation defines the polytope of interest, and it is the intersection of the two previous sets. Since Δ is the intersection of convex sets, then by construction it is also convex. For simplicity we assume all polytopes to be bounded, non-empty, and characterized with no redundant constraints.

2.2 Matrix multiplication

We adopt common notation used in matrix multiplication. ω represents the matrix multiplication coefficient - which characterizes the number of operations required to

multiply two $n \times n$ matrices. The complexity for such multiplication is of the order $\mathcal{O}(n^\omega)$. The lowest complexity for matrix multiplication algorithms is conjectured to be $\Omega(n^2)$ [Umans(2006)]. Table 1 shows the theoretical bounds for many well-known multiplication algorithms.

Table 1: Asymptotic complexity of matrix multiplication algorithms

Matrix Multiplication Algorithms	
Algorithm	**Complexity**
Naive	$\mathcal{O}(n^3)$
Strassen-Schonhaeg	$\mathcal{O}(n^{2.807})$
Coppersmith-Winograd	$\mathcal{O}(n^{2.376})$
Legall	$\mathcal{O}(n^{2.373})$

In general, [Knight(1995)] showed that the number of operations needed to multiply two matrices with dimensions $m \times n$ and $n \times p$ is of $\mathcal{O}(d_1 d_2 d_3^{\omega-2})$, where $d_3 = min\{m, n, p\}$ and $\{d_1, d_2\} = \{m, n, p\} - \{d_3\}$. The special case of matrix-vector multiplication $d_3 = 1$ yields a bound of $\mathcal{O}(mn)$. The smallest published ω is 2.373 legall$_m in$.

It is possible to define a function μ that represents the matrix multiplication order of complexity for matrices $A \in \mathbb{R}^{n_1 \times n_2}$ and $B \in \mathbb{R}^{n_2 \times n_3}$ as

$$\mu_{A,B} = \begin{cases} n_1^{\omega-2} n_2 n_3 & \text{if } \min\{n_1, n_2, n_3\} = n_1, \\ n_1 n_2^{\omega-2} n_3 & \text{if } \min\{n_1, n_2, n_3\} = n_2, \\ n_1 n_2 n_3^{\omega-2} & \text{if } \min\{n_1, n_2, n_3\} = n_3. \end{cases} \tag{4}$$

Thus we can express the complexity of the operation AB as $\mathcal{O}(\mu_{A,B})$.

In practice, only the Naive and Strassen's algorithms are used because the constants hidden in the Big O notation are usually significantly big for large enough matrices to take advantage of. Moreover, many multiplication algorithms are impractical due to numerical instabilities [Chen et al.(2018)Chen, Dwivedi, Wainwright, and Yu]. Fortunately, there have recently been fast and numerically stable implementations of the Strassen algorithm using GPUs ([Li et al.(2011)Li, Ranka, and Sahni], [Press et al.(2007)Press, Teukolsk

[Huang et al.(1993)Huang, Yu, and van de Geijn]).

3 HAR

This section explains the HAR algorithm and calculates its cost per iteration and mixing time for non-full dimensional polytopes, as defined in [Montiel and Bickel(2013a)].

3.1 Overview

HAR can be described as follows. A *walk* is initialized in a strict inner point of the polytope. At any iteration, a random direction is generated via independent normal variates. The random direction, along with the current point, generates a line set L, and its intersection with the polytope generates a line segment. The sampler selects a random point in L and repeats the process. After a warm start, HAR for full-dimensional convex bodies has a cost per iteration $\mathcal{O}(m_I n)$ and a cost per sample of $\mathcal{O}^*(m_I n^4)$ [Chen et al.(2018)Chen, Dwivedi, Wainwright, and Yu].

In general, the non-deterministic mixing time of HAR is of $\mathcal{O}^*(n^2 \gamma_\kappa)$, where γ_κ is defined as

$$\gamma_\kappa = \inf_{R_{in}, R_{out} > 0} \left\{ \frac{R_{out}}{R_{in}} \| \mathcal{B}(x, R_{in}) \subseteq \Delta \subseteq \mathcal{B}(y, R_{out}) \ for \ some \ x, y \in \Delta \right\},$$

where R_{in} and R_{out} are the radii of an inscribed and circumscribed ball of the polytope Δ, respectively, and $\mathcal{B}(q, R)$ is the ball of radius R containing the point q. In essence, γ_κ is the coefficient generated by the biggest inscribed ball and the smallest circumscribed ball of the polytope. That the mixing time depends on these parameters means that elongated polytopes are harder to sample. Implementations of HAR for convex bodies are typically analyzed after pre-processing and invoking a warm start, meaning that the body in question is brought to a near isotropic position in $\mathcal{O}^*(\sqrt{n})$, allowing the mixing time to be expressed as $\mathcal{O}^*(n^3)$ [Chen et al.(2018)Chen, Dwivedi, Wainwright, and Yu], [Lee and Vempala(2017)], [Lee and Vempala(2018)], [Lovász and Simonovits(1993)], [Lovász(1999)]

7

and [Tervonen et al.(2013)Tervonen, Valkenhoef, Basturk, and Postmus]. For ease of comparison with the literature, the remainder of the paper assumes that the polytope has received proper pre-processing.

A HAR sampler must compute the starting point and find the line segment L at each iteration. Additionally, a thinning factor (also called "burning rate") $\varphi(n)$ must be included to achieve a fair almost uniform distribution over the studied space [Tervonen et al.(2013)Tervonen, Valkenhoef, Basturk, and Postmus]. This means that after a warm start, the algorithm needs to drop $\varphi(n)$ sampled points for each desired i.i.d. observation. This thinning factor is known as the mixing-time, which is $\mathcal{O}^*(n^3)$ in the case of polytopes (see [Chen et al.(2018)Chen, Dwivedi, Wainwright, and Yu], [Tervonen et al.(2013)Tervonen, Valkenhoef, Basturk, and Postmus], [Lovász(1999)]).

The HAR pseudocode proposed in [Montiel and Bickel(2013a)] for full and non-full dimensional polytopes is presented in Algorithm 1. It samples a collection $\mathcal{X}$ of T uncorrelated points inside Δ. We know the complexity of HAR for full dimensional polytopes, to find the cost per iteration and cost per sample of HAR for non-full dimensional polytopes will require analyzing the complexity of calculating the projection matrix.

3.2 Projection matrix

The projection matrix P_{Δ^E} is computed from the equality matrix A^E. Then, P_{Δ^E} allows any vector to be projected to the null space of A^E. In our case, the random direction vector h lives in a full dimensional space, which means that if $m_E > 0$, h needs to be projected so that the line set L lives in the same space as Δ. The projection operation $P_{\Delta^E}h = d$ yields $A^E d = 0$. Then, $A^E(x + d) = b^E$ [Montiel and Bickel(2013a)]. (This step is omitted if $m_E = 0$.)

The projection matrix is defined as

$$P_{\Delta^E} = I - A'^E (A^E A'^E)^{-1} A^E. \tag{5}$$

8

Algorithm 1: HAR pseudocode

Result: $\mathcal{X}$

Initialization;

$t \leftarrow 0$ (Sample point counter);

$j \leftarrow 0$ (Iteration counter);

$\mathcal{X} = \emptyset$;

Set the total sample size T;

Set a thinning factor $\varphi(n)$;

Find a strictly inner point of the polytope Δ and label it $x_{t=0,j=0}$;

if $(m_E > 0)$ **then**
   | Compute the projection matrix P_{Δ^E}

end

while $t < T$ **do**
     Generate the direction vector $h \in \mathbb{R}^n$;
     if $(m_E = 0)$ **then**
       | $d = h$
     else
       | $d = P_{\Delta^E} h$
     end
     Find the line set $L := \{x | x = x_{t,j} + \theta d, x \in \Delta \ \& \ \theta \in \mathbb{R}\}$;
     $j \leftarrow j + 1$;
     Generate a point uniformly distributed in $L \cap \Delta$ and label it $x_{t,j+1}$;
     if $j == \varphi(n)$ **then**
         $\mathcal{X} = \mathcal{X} \cup x_{t,j}$;
         $t \leftarrow t + 1$;
         $j \leftarrow 0$;
     end

end

Lemma 3.1. *If $m_E < n$, then the complexity of calculating P_{Δ^E} is $\mathcal{O}(m_E^{\omega-2} n^2)$.*

Proof. Computing P_{Δ^E} is done in three matrix multiplications, one matrix-to-matrix subtraction, and one matrix inversion operation over $(A^E A'^E)$. The number of operations needed to calculate the inverse matrix depends on the algorithm used for matrix multiplication [Cormen et al.(2009)Cormen, Leiserson, Rivest, and Stein]. The order of number of operations for computing P_{Δ^E} is the sum of the following:

1. Obtain $(A^E A'^E)$ in $\mathcal{O}(\mu_{A^E, A'^E}) = \mathcal{O}(\mu(m_E, n, m_E)) = \mathcal{O}(m_E^{\omega-1} n)$ operations.

2. Find the inverse $(A^E A'^E)^{-1}$ in $\mathcal{O}(m_E^{\omega})$, since $(A^E A'^E)^{-1}$ has dimension $m_E \times m_E$.

175   3. Multiply $A'^E(A^E A'^E)^{-1}$ in $\mathcal{O}(\mu_{A'^E,(A^E A'^E)^{-1}}) = \mathcal{O}(\mu(n, m_E, m_E)) = \mathcal{O}(m_E^{\omega-1} n)$.

176   4. Calculate $A'^E(A^E A'^E)^{-1} A^E$ in $\mathcal{O}(\mu_{A'^E(A^E A'^E)^{-1}, A^E}) = \mathcal{O}(\mu(n, m_E, n)) = \mathcal{O}(m_E^{\omega-2} n^2)$.

177   5. Subtract $I - A'^E(A^E A'^E)^{-1} A^E$ in $\mathcal{O}(n^2)$.

178   These sum to $2 \times \mathcal{O}(m_E^{\omega-1} n) + \mathcal{O}(m_E^{\omega}) + \mathcal{O}(m_E^{\omega-2} n^2) + \mathcal{O}(n^2)$. Hence the complexity

179 of calculating P_{Δ^E} is $\mathcal{O}(\mu_{A'^E(A^E A'^E)^{-1}, A^E}) = \mathcal{O}(m_E^{\omega-2} n^2)$. $\square$

180   For simplicity, we will denote the complexity of computing P_{Δ^E} as $\mathcal{O}(\mu_{P_{\Delta^E}})$.

181 3.3   Non-full dimensional HAR

182 We proceed to calculate the cost per sample of HAR for $m_E > 0$. We start by computing

183 the cost per iteration in Lemma 3.2.

184 **Lemma 3.2.** *The cost per iteration of HAR for $0 \leq m_E$ is $\mathcal{O}(\max\{m_I n, m_E^{\omega-2} n^2\})$.*

185 *Proof.* As seen in Algorithm 1, the only difference between the full and non-full dimen-

186 sional cases is the projection step $P_{\Delta^E} h = d$. Then, the cost per iteration is defined by

187 the larger of the original cost per iteration $\mathcal{O}(m_I)$ of HAR for $m_E = 0$, and the extra

188 cost induced by the projection when $m_E > 0$.

189   Because P_{Δ^E} has dimension $n \times n$ and h is an $n \times 1$ vector, $\mu_{P_{\Delta^E}, h} = n^2$ and

190 the complexity is $\mathcal{O}(n^2)$. By Lemma 3.1, finding P_{Δ^E} has an asymptotic complex-

191 ity of $\mathcal{O}(m_E^{\omega-2} n^2)$. Therefore, the cost of projecting h at each iteration is $\mathcal{O}(n^2) +$

192 $\mathcal{O}(m_E^{\omega-2} n^2) = \mathcal{O}(m_E^{\omega-2} n^2)$, since $m_E > 0$. Therefore, the cost per iteration for $m_E > 0$

193 is $\mathcal{O}(\max\{m_I n, m_E^{\omega-2} n^2)\})$. If $m_E = 0$, then the coefficient $\max\{m_I n, m_E^{\omega-2} n^2\}$ equals

194 $\max\{m_I n, 0\} = m_I n$ and the cost per sample is $\mathcal{O}^*(\max\{m_I n, 0\}\}) = \mathcal{O}^*(m_I n)$. $\square$

195   Having calculated the cost per iteration of HAR, we can proceed to Theorem 3.3.

196 **Theorem 3.3.** *The cost per sample of HAR for $0 \leq m_E$ is $\mathcal{O}^*(n^3 \max\{m_I n, m_E^{\omega-2} n^2\})$*

197 *after proper pre-processing and a warm start.*

Proof. According to [Chen et al.(2018)Chen, Dwivedi, Wainwright, and Yu], the cost per sample of a sampling algorithm is its mixing time complexity multiplied by its cost per iteration. By Lemma 3.2, the cost per iteration is $\mathcal{O}(\max\{m_I n, m_E^{\omega-2} n^2\})$. Moreover, [Tervonen et al.(2013)Tervonen, Valkenhoef, Basturk, and Postmus] states that the mixing time, after a warm start, of HAR is $\mathcal{O}^*(n^3)$. Therefore, the cost per sample is $\mathcal{O}^*(n^3 \max\{m_I n, m_E^{\omega-2} n^2\})$.

Recall that if $m_E = 0$ the *cost per sample* is $\mathcal{O}^*(n^3 \max\{m_I n, 0\}) = \mathcal{O}^*(m_I n^4)$ that is the special case of HAR for full dimensional polytopes. $\qquad\square$

4   Matrix Hit-and-Run (MHAR)

This section details our new algorithm, Matrix Hit-And-Run (**MHAR**). MHAR has a lower cost per sample than does HAR. Furthermore, making z simultaneous walks with MHAR requires fewer operations than does running z HAR walks in parallel. The "padding" hyper-parameter z allows the concatenation of multiple directions d and samples x to form matrices D and $\mathcal{X}$, respectively. Each column of these matrices represents a walk over the polytope. This modification permits the use of efficient matrix-to-matrix operations to simultaneously project many directions d and find their respective line segments.

4.1   MHAR preliminaries

MHAR explores the polytope using simultaneous walks by drawing multiple directions d from the n-dimensional hypersphere. Each independent walk has the same mixing-time as with HAR, but a lower cost per iteration. Instead of running separate threads, we "batch" the walks by "padding" vector x and d with z columns, creating the matrices $X = (x^1 | \ldots | x^k | \ldots | x^z)$ and $D = (d^1 | \ldots | d^k | \ldots | d^z)$. Super index k denotes the kth walk represented by the kth column in the padded matrix. The algorithm then adapts the steps in HAR to keep track of each independent walk and recast the operations as

11

matrix-to-matrix. The algorithm is tailored for exploiting cutting-edge matrix routines that exploit the architectures of machines like GPUs, cache memories, and multiple cores.

The main difference with HAR when running z instances on multiple independent cores (z-HAR) is the estimation of $D = (d^1 | \ldots | d^k | \ldots | d^z)$ and the line segments L^k in a simultaneous fashion for all z-walks. In both, z-HAR and MHAR, each walk is oblivious of the others after a warm start, which guarantee a constant mixing-time among all z-walks [Montiel and Bickel(2013a)] [Lovász and Vempala(2006)].

Algorithm 2 presents the pseudocode for MHAR.

4.2 Starting point

In general, the cost of finding the starting point is excluded from the complexity analysis because it is independent of the mixing-time. However, we present it here for completeness even though the literature assumes a warm start in determining cost per sample ([Chen et al.(2018)Chen, Dwivedi, Wainwright, and Yu], [Tervonen et al.(2013)Tervonen, Valkenhoef, E [Lee and Vempala(2018)]).

MHAR needs to be initialized by a point in the relative interior of the polytope. We suggest Chebyshev's center of the polytope, which is the center of the largest inscribed ball. For polytopes, Chebyshev's center can be formulated as a linear optimization problem and solved using standard methods.

Chebyshev's center is presented in Model (6).

$$
\begin{aligned}
&\max_{x \in \mathbb{R}^n, r \in \mathbb{R}} r, \\
&s.t \quad A^E x = b^E, \\
&(a_i^I)^T x + r||a_i^I||_2 \leq b_i^I, \ \forall i = 1, ..., m_I,
\end{aligned}
\tag{6}
$$

where a_i^I and b_i^I represent the ith row of matrix A^I and ith entry from vector b^I, respectively. Model (6) has the original m restrictions plus one additional variable r.

Algorithm 2: MHAR pseudocode

Result: $\mathcal{X}$

Initialization;

$t \leftarrow 0$ (Sample point counter);

$j \leftarrow 0$ (Iteration counter);

$z \leftarrow \max\{m_I, n\} + 1$;

$\mathcal{X} = \emptyset$;

Set the total sample size T;

Set a thinning factor $\varphi(n)$;

Find a strictly inner point of the polytope Δ and label it $x_{t,j}$;

Set $x_{t,j}^k = x_{t,j}, \ \forall k \in \{1, ..., z\}$;

Initialize $X_{t,j} = (x_{t,j}^1|...|x_{t,j}^k|...|x_{t,j}^z) \in \mathbb{R}^{n \times z}$;

if $(m_E > 0)$ **then**
$\quad \lfloor$ Compute the projection matrix P_{Δ^E}

while $t < T$ **do**
$\quad$ **Generate** $H = (h^1|...|h^k|...|h^z) \in \mathbb{R}^{n \times z}$, the direction matrix;
$\quad$ **if** $(m_E = 0)$ **then**
$\quad\quad |\quad D = H$;
$\quad$ **else**
$\quad\quad \lfloor\quad D = P_{\Delta^E} H = (d^1|...|d^k|...|d^z)$;
$\quad$ **Find** the line sets $\left\{ L^k := \{x | x = x_{t,j}^k + \theta^k d^k, \ x \in \Delta \ \& \ \theta^k \in \mathbb{R}\} \right\}_{k=1}^z$;
$\quad$ $j \leftarrow j + 1$;
$\quad$ **Generate** a point uniformly distributed in each L^k and label it $x_{t,j}^k$ in $X_{t,j}$;
$\quad$ **if** $j == \varphi(n)$ **then**
$\quad\quad |\quad \mathcal{X} = \mathcal{X} \cup \{x_{t,j}^1, ..., x_{t,j}^z\}$;
$\quad\quad |\quad t \leftarrow t + z$;
$\quad\quad \lfloor\quad j \leftarrow 0$;

245 Hence, the size of the problem has m constraints and $n+1$ variables. Then, calculating

246 the $|| \cdot ||_2$ coefficients takes $\mathcal{O}(mn)$. Thus, it can be formulated and solved in $\mathcal{O}(n^\omega)$

247 using Vaidya's algorithm [Vaidya(1989)] for linear optimization. After solving Model

248 (6), we use x as the starting point $x_{t=0, j=0}$ for all walks and draw independent walking

249 directions. The matrix $X_{t,j} \in \mathbb{R}^{n \times z}$ introduced in Algorithm 2 is the algorithmic version

250 of X, and it summarizes the state of all walks, where each kth column represents the

251 current point of walk k at iteration $\{t, j\}$. Formally we say $X_{t,j} = (x_{t,j}^1|...|x_{t,j}^k|...|x_{t,j}^z)$

252 where $x_{t,j}^k \in \mathbb{R}^{n \times 1} \ \forall k \in \{1, ..., z\}$.

4.3 Generating D

Because the target distribution of HAR and MHAR is uniform, we follow the procedure established in [Montiel and Bickel(2013a)] and [Lovász(1999)] that uses the Margsalia method [Marsaglia(1972)] to generate a random vector h from the hypersphere by generating n i.i.d. samples from a standard normal distribution $\mathcal{N}(0, 1)$. However, instead of generating a single direction vector $d \in \mathbb{R}^n$, we create matrices $H, D \in \mathbb{R}^{n \times z}$, where each element of the matrix corresponds to an independent execution of the Box-Muller method [Chay et al.(1975)Chay, Fardo, and Mazumdar] bounded by $\mathcal{O}(nz)$. If the polytope is full dimensional, $H = D$ and no projection operation is needed. Otherwise, the projection matrix P_{Δ^E} is calculated as in §3, and Lemma 3.1 bounds the number of operations as $\mathcal{O}(m_E^{\omega-2} n^2)$.

Matrices H and D can be visualized as

$$H = (h^1|...|h^k|...|h^z), \ h^k \in \mathbb{R}^n, \ \forall k \in \{1, ..., z\}, \tag{7}$$

$$D = P_{\Delta^E} H = (d^1|...|d^k|...|d^z), \ d^k \in \mathbb{R}^n, \ \forall k \in \{1, ..., z\}. \tag{8}$$

Each column h^k can be projected by the operation $D = P_{\Delta^E} H$. Hence, each column of D satisfies the restrictions in Δ^E and serves as a direction d for an arbitrary walk k. In principle, z can be any number in $\mathbb{N}$, where $z = 1$ is the special case that recovers the original HAR.

Lemma 4.1. *The complexity of generating matrix D in MHAR given P_{Δ^E} and $\max\{m_I, n\} \leq z$ is $\mathcal{O}(nz)$ if $m_E = 0$, and $\mathcal{O}(n^{\omega-1} z)$ if $m_E > 0$.*

Proof. Generating H has complexity $\mathcal{O}(nz)$ using the Box-Muller method. If $m_E = 0$, then $D = H$, implying a total asymptotic cost $\mathcal{O}(nz)$. If $m_E > 0$, then $D = P_{\Delta^E} H$, whose cost $\mathcal{O}(\mu_{P_{\Delta^E}, H}) = \mathcal{O}(n^{\omega-1} z)$ given by $\max\{m_I, n\} \leq z$, needs to be included. $\mathcal{O}(n^{\omega-1} z)$ bounds $\mathcal{O}(nz)$. Therefore, the total cost of computing D for $m_E > 0$ is bounded by $\mathcal{O}(n^{\omega-1} z)$. $\qquad \square$

Lemma 4.1 shows that if $m_E > 0$, the cost of generating new directions d does not

14

scale as if had used z parallel HARs. In the HAR case, the operations required would have been carried out in $\mathcal{O}(z\mu_{P_{\Delta E},h}) = \mathcal{O}(zn^2)$, averaging $\mathcal{O}(\frac{zn^2}{z}) = \mathcal{O}(n^2)$ per direction. In contrast, MHAR is $\mathcal{O}(n^{\omega-1}z)$, averaging $\mathcal{O}(\frac{n^{\omega-1}z}{z}) = \mathcal{O}(n^{\omega-1})$ per direction. When $m_E = 0$, the number of operations for both cases is the same.

4.4 Finding the line sets

Given matrices X and D, we now obtain the line sets $\{L^k\}_{k=1}^z$:

$$\left\{ L^k := \{x | x = x^k + \theta^k d^k, \ x \in \Delta, \text{ and } \theta^k \in \mathbb{R}\} \right\}_{k=1}^z. \tag{9}$$

Each θ^k characterizes the line set for column x^k. The "padded" column-wise representation of restrictions Δ^I is

$$A^I X = \begin{pmatrix} a_1^I x^1 & \cdots & a_1^I x^k \\ \vdots & \ddots & \vdots \\ a_{m_I}^I x^1 & \cdots & a_{m_I}^I x^k \end{pmatrix} \leq \begin{pmatrix} b_1^I \\ \vdots \\ b_{m_I}^I \end{pmatrix} = b^I, \tag{10}$$

where each element from the left matrix must be less than or equal to the corresponding element (row-wise) in vector b^I. The restrictions for an arbitrary x^k can be rewritten row-wise so that the left side and right side are scalars:

$$a_i^I x^k \leq b_i^I, \ \forall i \in \{1, \ldots, m_I\}. \tag{11}$$

Then, each θ^ks must satisfy

$$(a_i^I x^k + \theta^k a_i^I d^k) < b_i^I, \ \forall i \in \{1, \ldots, m_I\}. \tag{12}$$

Rearranging the terms obtains restrictions for each walk k, where each θ^k must be

15

bounded by its respective set of lambdas $\{\lambda_i^k\}_{i=1}^{m_I}$, as follows:

$$\theta^k < \lambda_i^k = \frac{b_i^I - a_i^I x^k}{a_i^I d^k}, \quad if \ a_i^I d^k > 0, \tag{13}$$

$$\theta^k > \lambda_i^k = \frac{b_i^I - a_i^I x^k}{a_i^I d^k}, \quad if \ a_i^I d^k < 0. \tag{14}$$

Hence, a walk's boundaries are represented by

$$\lambda_{min}^k = \max \ \{\lambda_i^k \mid a_i^I d^k < 0\}, \tag{15}$$

$$\lambda_{max}^k = \min \ \{\lambda_i^k \mid a_i^I d^k > 0\}. \tag{16}$$

These lambdas can be used to construct the intervals $\Lambda^k = (\lambda_{\min}^k, \lambda_{\max}^k)$, $k \in \{1, ..., z\}$. By construction, if $\theta^k \in \Lambda^k$ and $x^k \in \Delta$, then $x^k + \theta^k d^k \in L^k$, since $A^I(x^k + \theta^k d^k) \le b^I$ and $A^E(x^k + \theta^k d^k) = b^E$. The line segment can be found simply by evaluating $\{\Lambda^k\}_{k=1}^z$, because x^k and D were computed previously. We can now state Lemma 4.2.

Lemma 4.2. *The complexity of generating all line sets $\{L^k\}_{k=1}^z$ in MHAR given D, X, and $\max\{m_I, n\} \le z$ is bounded by $\mathcal{O}(m_I n^{\omega-2} z)$ if $n \le m_I$, and by $\mathcal{O}(m_I^{\omega-2} n z)$ otherwise.*

Proof. All Λ^ks can be obtained as follows:

1. Obtain matrix $A^I X$ in $\mathcal{O}(\mu_{A^I,X})$. This is done in $\mathcal{O}(m_I n^{\omega-2} z)$ if $n \le m_I$, and in $\mathcal{O}(m_I^{\omega-2} n z)$ otherwise.

2. Compute $B^I - A^I X$, where $B_I = (b^I|...|b^I) \in \mathbb{R}^{m_I \times z}$, which takes $\mathcal{O}(m_I z)$ operations.

3. Calculate $A^I D$, which is bounded by $\mathcal{O}(\mu_{A^I,D})$, which is done in $\mathcal{O}(m_I n^{\omega-2} z)$ *if* $n \le m_I$, and in $\mathcal{O}(m_I^{\omega-2} n z)$ otherwise.

4. Divide $\frac{B^I - A^I X}{A^I D}$ (entry-wise) to obtain all λ_i^k. All the necessary point-wise operations for this calculation have a combined order of $\mathcal{O}(m_I z)$.

16

5. For each $k \in \{1, ..., z\}$, find which coefficients $a_i^I d^k$ are positive or negative, which takes $\mathcal{O}(m_I z)$.

6. For each $k \in \{1, ..., z\}$, find the intervals $\lambda_{min}^k = \max \{\lambda_i^k \mid a_i^I d^k < 0\}$ and $\lambda_{max}^k = \min \{\lambda_i^k \mid a_i^I d^k > 0\}$, which can be done in $\mathcal{O}(m_I z)$.

This procedure constructs all the intervals $\Lambda^k = (\lambda_{\min}^k, \lambda_{\max}^k)$. The complexity of this operation is bounded by $\mathcal{O}(\mu_{A^I,X}) = \mathcal{O}(\mu_{A^I,D})$. Hence, the complexity of finding all line sets is bounded by $\mathcal{O}(m_I n^{\omega-2} z)$ *if* $n \leq m_I$, and by $\mathcal{O}(m_I^{\omega-2} n z)$ otherwise. $\square$

Lemma 4.2 bounds the complexity of finding the line sets at any iteration of MHAR. This leaves only analyzing the cost of choosing a new sample.

4.5   Choosing samples

The following lemma bounds the complexity of choosing a new $X_{t,j+1}$ or $X_{t+z,0}$ given $\Lambda^k \; \forall k \in \{1, ..., z\}$. The new samples will be padded to create the matrix $X_{t,j+1} = (x_{t,j+1}^1 | \ldots | x_{t,j+1}^k)$ to be used in the next iteration.

Lemma 4.3. *Sampling z new points given $\{\Lambda^k\}_{k=1}^z$ has complexity $\mathcal{O}(zn)$.*

Proof. Selecting a random $\theta^k \in \Lambda^k$ takes $\mathcal{O}(1)$. Sampling a new point $x_{t,j+1}^k = x_{t,j}^k + \theta d_{t,j}^k$ has complexity $\mathcal{O}(n)$ because it requires n scalar multiplications and n sums. Then, sampling all new $x_{t,j+1}^k$ points is bounded by $\mathcal{O}(zn)$. $\square$

Having concluded the complexity analysis for each step of the loop, we next calculate the cost per iteration and proceed to measure the cost per sample.

4.6   Iteration and sampling costs of MHAR

The asymptotic behavior of each operation that comprises the main loop of MHAR when $\max\{n, m_I\} \leq z$ is presented in Table 2. The cost of finding the starting point is excluded ([Chen et al.(2018)Chen, Dwivedi, Wainwright, and Yu], [Tervonen et al.(2013)Tervonen, Valken

17

Table 2: Asymptotic cost per sample of MHAR at each step

MHAR complexity at each step, $(n, m) < z$				
Operation	$m_E = 0,$ $n \leq m_I.$	$m_E = 0,$ $n > m_I.$	$m_E > 0,$ $n \leq m_I.$	$m_E > 0,$ $n > m_I.$
1.Projection matrix	$\mathcal{O}(1)$	$\mathcal{O}(1)$	$\mathcal{O}(m_E^{\omega-2}n^2)$	$\mathcal{O}(m_E^{\omega-2}n^2)$
2.Generating D	$\mathcal{O}(nz)$	$\mathcal{O}(nz)$	$\mathcal{O}(n^{\omega-1}z)$	$\mathcal{O}(n^{\omega-1}z)$
3.Finding $\{L^k\}_{k=1}^z$	$\mathcal{O}(m_I n^{\omega-2}z)$	$\mathcal{O}(m_I^{\omega-2}nz)$	$\mathcal{O}(m_I n^{\omega-2}z)$	$\mathcal{O}(m_I^{\omega-2}nz)$
4.Sampling all $x_{t,j+1}^k$	$\mathcal{O}(nz)$	$\mathcal{O}(nz)$	$\mathcal{O}(nz)$	$\mathcal{O}(nz)$

The following lemmas will help bound the cost per iteration of MHAR. Lemmas 4.4 and 4.5 establish the full dimensional case for $(n \leq m_I)$ and $(n > m_I)$, respectively. Lemmas 4.8 and 4.9 do likewise in the non-full dimensional case for $(n \leq m_I)$ and $(n > m_I)$, respectively.
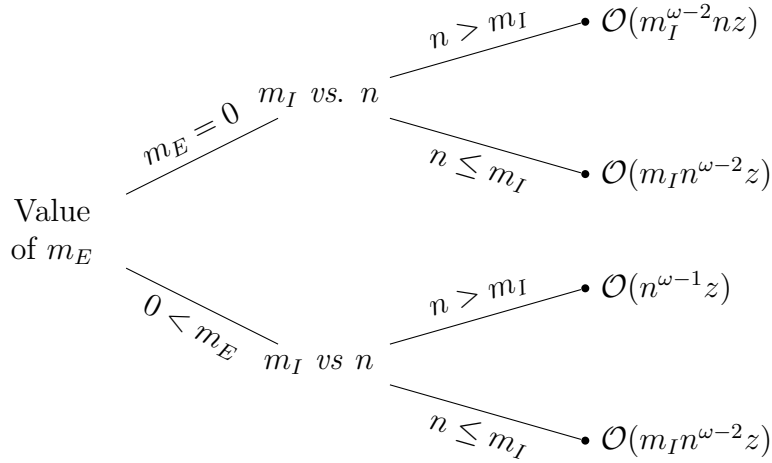
Figure 1 summarizes these results as follows.

Figure 1: Asymptotic behavior of the cost per iteration of MHAR.

Lemma 4.4. *Assume $m_E = 0$, $\max\{n, m\} < z$, and $n \leq m_I$. Then, the cost per iteration of MHAR is $\mathcal{O}(m_I n^{\omega-2}z)$, which is the number of operations needed for finding all line sets $\{L^k\}_{k=1}^z$.*

18

Proof. First we enumerate the cost of each step of the iteration for $m_E = 0$ and $n \leq m_I$ if $\max\{n, m\} < z$:

1. By Lemma 3.1, generating P_{Δ^E} is bounded by $\mathcal{O}(1)$.

2. By Lemma 4.1, generating D is bounded by $\mathcal{O}(nz)$.

3. By Lemma 4.2, generating $\{L^k\}_{k=1}^z$ for $n \leq m_I$ is bounded by $\mathcal{O}(m_I n^{\omega-2} z)$.

4. By Lemma 4.3, generating all new $x_{t,j+1}^k$ is bounded by $\mathcal{O}(zn)$.

By hypothesis, $0 < n \leq m_I$. Then, $nz \leq m_I z < m_I n^{\omega-2} z$, because $\omega \in (2,3]$. Therefore, $\mathcal{O}(1) \subseteq \mathcal{O}(nz) \subseteq \mathcal{O}(m_I n^{\omega-2} z)$, where the first term is the complexity of finding the projection matrix (omitted for $m_E = 0$), the second one bounds generating D and sampling new points, and the third one is the asymptotic cost of finding all line sets $\{L^k\}_{k=1}^z$. $\qquad\square$

Lemma 4.5. *Assume $m_E = 0$, $\max\{n, m\} < z$, and $n > m_I$. Then, the cost per iteration of MHAR is $\mathcal{O}(n m_I^{\omega-2} z)$, which is the number of operations needed for finding all line sets $\{L^k\}_{k=1}^z$.*

Proof. As in the proof of Lemma 4.4, the complexity of the projection matrix, generating D, and sampling all new $x_{t,j+1}^k$ points is the same, given by $m_E = 0$ and $n > m_I$. Hence, the only change is provided by Lemma 4.2, in which the cost of finding all line sets $\{L^k\}_{k=1}^z$ for $n > m_I$ is $\mathcal{O}(n m_I^{\omega-2} z)$. By hypothesis, $0 < m_I$ and $\max\{n, m\} < z$, thus $nz < n m_I^{\omega-2} z$. Therefore, $\mathcal{O}(1) \subseteq \mathcal{O}(nz) \subseteq \mathcal{O}(n m_I^{\omega-2} z)$, where the third term is the cost of finding all line sets $\{L^k\}_{k=1}^z$. $\qquad\square$

Corollary 4.6. *Assume $m_E = 0$ and $\max\{n, m\} < z$. Then, the cost per iteration of MHAR is bounded by the cost of finding all line sets $\{L^k\}_{k=1}^z$.*

Proof. The proof follows from Lemmas 4.4 and 4.5. $\qquad\square$

We proceed to finding the cost per iteration for the non-full dimensional case $m_E > 0$.

Lemma 4.7. *Assume $m_E < n$ and $(m, n) < z$. Then, the cost of calculating the projection matrix P_{Δ^E} is bounded by the cost of generating D.*

Proof. By hypothesis $m_E < n$, implying that $m_E^{\omega-2} n^2 < n^{\omega-2} n^2 = n^{\omega}$. Because $n < z$, $n^{\omega} = n^{\omega-1} n < n^{\omega-1} z$. Combining both inequalities yields $m_E^{\omega-2} n^2 < n^{\omega} < n^{\omega-1} z$. Therefore, $\mathcal{O}(m_E^{\omega-2} n^2) \subseteq \mathcal{O}(n^{\omega-1} z)$, where the first term is the complexity of computing P_{Δ^E} (by Lemma 3.1), and the second term is the complexity of projecting H in order to obtain D (by Lemma 4.1). $\square$

Lemma 4.8. *Assume $m_E > 0$, $\max\{n, m\} < z$, and $n \leq m_I$. Then, the cost per iteration of MHAR is $\mathcal{O}(m_I n^{\omega-2} z)$, which is the number of operations needed for finding all line sets $\{L^k\}_{k=1}^z$.*

Proof. First, we enumerate the cost of each step of the iteration for $m_E > 0$, $n \leq m_I$, and $\max\{n, m\} < z$:

1. By Lemma 3.1, generating P_{Δ^E} is bounded by $\mathcal{O}(m_E^{\omega-2} n^2)$.

2. By Lemma 4.1, generating D is bounded by $\mathcal{O}(n^{\omega-1} z)$.

3. By Lemma 4.2, generating $\{L^k\}_{k=1}^z$ for $n \leq m_I$ is bounded by $\mathcal{O}(m_I n^{\omega-2} z)$.

4. By Lemma 4.3, generating all new $x_{t,j+1}^k$ is bounded by $\mathcal{O}(zn)$.

Using Lemma 4.7, the Big-O term for finding P_{Δ^E} (step 1) is bounded by the term of generating D (step 2). Because $n < m_I$, $n^{\omega-1} z = n^{\omega-2} n z < n^{\omega-2} m_I z$. Therefore, $\mathcal{O}(m_E^{\omega-2} n^2) \subseteq \mathcal{O}(n^{\omega-1} z) \subseteq \mathcal{O}(m_I n^{\omega-2} z)$, which are the respective costs of steps 1, 2, and 3. Furthermore, $nz \leq n^{\omega-2} m_I z$, implying that step 4 is also bounded by step 3 in terms of complexity. This implies that all the operations above are bounded by the term $\mathcal{O}(m_I n^{\omega-2} z)$, which is the asymptotic complexity of finding all line sets $\{L^k\}_{k=1}^z$. $\square$

Lemma 4.9. *Assume $m_E > 0$, $\max\{n, m\} < z$, and $n > m_I$. Then, the cost per iteration of MHAR is $\mathcal{O}(n m_I^{\omega-2} z)$, which is the number of operations needed for generating D.*

20

$_{381}$ *Proof.* As in the proof of Lemma 4.8, the cost of the projection matrix, generating D,

$_{382}$ and sampling all new $x_{t,j+1}^k$ points is the same, given by $m_E > 0$ and $n > m_I$. Hence,

$_{383}$ the only change is provided by Lemma 4.2, in which the cost of finding all line sets

$_{384}$ $\{L^k\}_{k=1}^z$ for $n > m_I$ is $\mathcal{O}(nm_I^{\omega-2}z)$.

$_{385}$ By Lemma 4.7, the Big-O term for finding P_{Δ^E} is bounded by the term of gen-

$_{386}$ erating D. Because $n > m_I$, $m_I^{\omega-2}nz < n^{\omega-2}nz = n^{\omega-1}z$. Therefore, $\mathcal{O}(m_E^{\omega-2}n^2) \subseteq$

$_{387}$ $\mathcal{O}(nm_I^{\omega-2}z) \subseteq \mathcal{O}(n^{\omega-1}z)$, which are the respective costs of the projection matrix, find-

$_{388}$ ing all line sets, and generating D. Furthermore, $nz \leq n^{\omega-2}nz = n^{\omega-1}z$, implying that

$_{389}$ the cost of sampling all new $x_{t,j+1}^k$ is also bounded by the cost of generating D. This

$_{390}$ implies that all the operations above are bounded by $\mathcal{O}(nm_I^{\omega-2}z)$. $\square$

$_{391}$ We can now proceed to the main results of the paper, given in Theorem 4.10.

$_{392}$ **Theorem 4.10.** *If* $\max\{n, m\} < z$, *then after proper pre-processing and a warm start,*

$_{393}$ *the cost per sample of MHAR is*

$$
\begin{cases}
\mathcal{O}^*(m_I n^{\omega+1}), & if \ m_E = 0 \ and \ n \leq m_I \\
\mathcal{O}^*(n^{\omega+2}), & if \ m_E = 0 \ and \ n > m_I \\
\mathcal{O}^*(m_I n^{\omega+1}), & if \ m_E > 0 \ and \ n \leq m_I \\
\mathcal{O}^*(m_I^{\omega-2} n^4), & if \ m_E > 0 \ and \ n > m_I.
\end{cases}
\tag{17}
$$

$_{394}$ *Proof.* Lemmas 4.4, 4.5, 4.8, and 4.9 gave the cost per iteration of MHAR for all four

$_{395}$ cases:

$$
\begin{cases}
\mathcal{O}(m_I n^{\omega-2}z), & if \ m_E = 0 \ and \ n \leq m_I \\
\mathcal{O}(n^{\omega-1}z), & if \ m_E = 0 \ and \ n > m_I \\
\mathcal{O}(m_I n^{\omega-2}z), & if \ m_E > 0 \ and \ n \leq m_I \\
\mathcal{O}(m_I^{\omega-2} nz), & if \ m_E > 0 \ and \ n > m_I.
\end{cases}
\tag{18}
$$

$_{396}$ It was stated that each walk from the "padding" is independent about the other

ones after a warm-start. Then, each individual walk has a mixing time of $\mathcal{O}^*(n^3)$. Then it suffices to apply the rule for Big-O products between the cost per iteration and the mixing time, and divide the coefficient by the padding parameter z, which is the number of points obtained at each iteration. Hence, multiplying each case in Equation (18) by $\frac{n^3}{z}$ obtains the desired result. $\square$

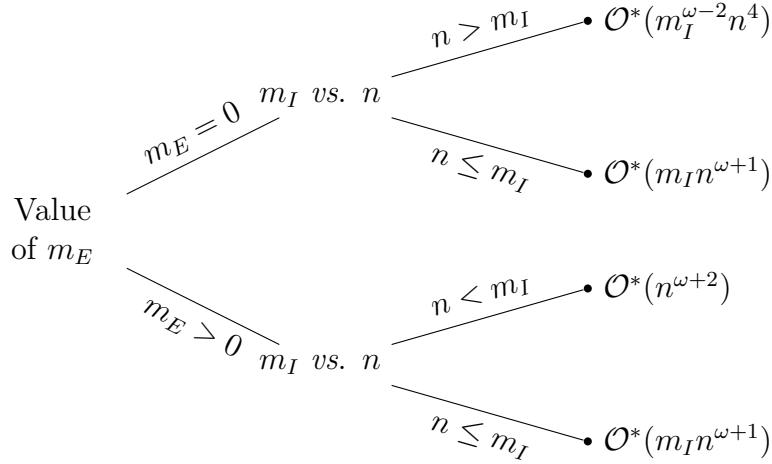Figure 2 graphically depicts the results of the theorem.

Figure 2: Asymptotic behavior of the cost per sample of MHAR after a warm start.

Theorem 4.10 characterizes the cost per sample of MHAR for all parameter values. The theorem shows that MHAR is always at least as efficient as HAR, and more efficient for $\omega \in (2, 3)$. Intuitively this is caused by "padding," which permits matrix-to-matrix multiplications instead of isolated matrix-to-vector operations when finding the line sets L or the directions D. Furthermore, this approach allows efficient cache usage and state-of-the-art GPU matrix multiplication algorithms.

5   MHAR Complexity Benchmarks

This section benchmarks the asymptotic behavior of MHAR against that for seven state-of-the-art algorithms. Some of these algorithms cover additional convex figures, like

22

spheres or cones. However, we restrict our focus on polytopes because they are the target of MHAR. For in-depth analysis of each algorithm, see [Chen et al.(2018)Chen, Dwivedi, Wainwright, We prioritize the full-dimensional case ($m = m_I, m_E = 0$) because few algorithms are designed for the non-full dimensional scenario and their analysis is outside our scope. Table 3 is adapted from [Chen et al.(2018)Chen, Dwivedi, Wainwright, and Yu] and includes the notation established in [Tervonen et al.(2013)Tervonen, Valkenhoef, Basturk, and Postmus] and [Montiel and Bickel(2013a)]. The authors of RHCM [Lee and Vempala(2018)], John's walk [Gustafson and Narayanan(2018)], Vaidya walk, and John walk omitted $m < n$, which is also outside of our scope. Note that John's walk and John walk are different algorithms.

In §4 we showed that the MHAR has lower cost per sample than the HAR for efficient matrix multiplication algorithms. Furthermore, because the Ball walk [Lovász and Simonovits(1993)] has the same cost per sample as HAR, we can derive the next corollary.

Corollary 5.1. *The cost per sample of MHAR is as low as the cost per sample of the Ball walk, after a warm start, if $\max\{n, m\} < z$. And strictly lower if efficient matrix-to-matrix algorithms are used $\big(\omega \in (2, 3)\big)$.*

Proof. This follows from comparing Theorem 4.10 against the complexity of the Ball walk. □

The following lemma shows that MHAR has a lower cost per sample than does John's walk.

Lemma 5.2. *For $\max\{n, m\} < z$, and $n < m$, MHAR has a lower cost per sample than does John's walk after proper pre-processing, warm start, and ignoring the logarithmic and error terms.*

Proof. Given proper pre-processing, $n \ll m$, and $\max\{n, m\} < z$, then MHAR's cost per sample is $\mathcal{O}^*(mn^{\omega+1})$, and that for John's walk is $\mathcal{O}(mn^{11} + n^{15})$. Note that $mn^{\omega+1} \in \mathcal{O}(mn^{11} + n^{15})$. Therefore, when ignoring the logarithmic and error terms, MHAR has a lower cost per sample. □

23

Table 3: Asymptotic behavior of random walks

Random walks behaviour			
Walk	**Mixing time**	**Cost per iteration**	**Cost per sample**
MHAR with $n > m$	n^3	$m^{\omega-2}nz$	$m^{\omega-2}n^4$
MHAR with $n \leq m$	n^3	$mn^{\omega-2}z$	$mn^{\omega+1}$
Ball walk	n^3	mn	mn^4
HAR	n^3	mn	mn^4
Dikin walk with $n \leq m$	mn	$mn^{\omega-1}$	m^2n^{ω}
RHCM with $n \leq m$	$mn^{\frac{2}{3}}$	$mn^{\omega-1}$	$m^2n^{\omega-\frac{1}{3}}$
John's walk with $n \leq m$	n^7	$mn^4 + n^8$	$mn^{11} + n^{15}$
Vaidya walk with $n \leq m$	$m^{\frac{1}{2}}n^{\frac{3}{2}}$	$mn^{\omega-1}$	$m^{1.5}n^{\omega+\frac{1}{2}}$
John walk with $n \leq m$	$n^{\frac{5}{2}}log^4(\frac{2m}{n})$	$mn^{\omega-1}log^2(m)$	$mn^{\omega+\frac{3}{2}}$

The table contains the upper bounds on the cost per sample (after a warm start) for various random walk algorithms applied to polytopes. In the case of MHAR, $\max\{n, m\} < z$ is assumed. For simplicity, we ignore the logarithmic terms in the cost per sample. We also avoid giving bounds in terms of the condition number of the set for MHAR, Ball walk, and HAR, because this condition number is bounded by n after proper pre-processing.

In the regime of $n \ll m$, the overall upper bound complexity for the cost per sample is represented by John walk $\ll$ Vaidya walk $\ll$ Dikin walk [Chen et al.(2018)Chen, Dwivedi, Wainwright, We now show that for $n \ll m$, MHAR has a lower cost per sample than does John walk.

Lemma 5.3. *For $\max\{n, m\} < z$ and the regime $n \ll m$, MHAR has a lower cost per sample than does the John walk after proper pre-processing, warm start, and ignoring logarithmic and error terms.*

Proof. From proper pre-processing, $n \ll m$, and $\max\{n, m\} < z$, MHAR's cost per sample is $\mathcal{O}^*(mn^{\omega+1})$ and that for John walk is $\mathcal{O}(mn^{\omega+\frac{3}{2}})$. Note that $mn^{\omega+1} \in \mathcal{O}(mn^{\omega+\frac{3}{2}})$. Therefore when ignoring the logarithmic and error terms, MHAR has

a lower cost per sample. □

Corollary 5.4. *For* $\max\{n, m\} < z$ *and the regime* $n \ll m$*, then MHAR* $\ll$ *John Walk* $\ll$ *Vaidya walk* $\ll$ *Dikin walk after proper pre-processing, warm start, and ignoring logarithmic and error terms.*

Proof. This follows from Lemma 5.3. □

We proceed to compare MHAR and RHMC for the regime $n^{1+\frac{1}{3}} \ll m$.

Lemma 5.5. *For* $\max\{n, m\} < z$ *and* $n^{1+\frac{1}{3}} \ll m$*, then MHAR* $\ll$ *RHMC after proper pre-processing, warm start and ignoring logarithmic and error terms.*

Proof. From proper pre-processing, $n \ll m$, and $n, m < z$, MHAR's cost per sample is $\mathcal{O}^*(mn^{\omega+1})$, and RHMC's is $\mathcal{O}(m^2 n^{\omega-\frac{1}{3}})$. Note that $mn^{\omega+1} \in \mathcal{O}(m^2 n^{\omega-\frac{1}{3}})$, because $n^{1+\frac{1}{3}} \ll m$. Therefore, when ignoring the logarithmic and error terms, MHAR has a lower cost per sample. □

From corollaries 5.1 and 5.2, MHAR $\ll$ Ball walk and MHAR $\ll$ HAR, regardless of the regime between m and n. And MHAR $\ll$ John's Walk for the regime $n \leq m$. From corollary 5.4, MHAR $\ll$ John Walk $\ll$ Vaidya walk $\ll$ Dikin walk if $n < m$. Finally, by Lemma 5.5, if $n^{1+\frac{1}{3}} \ll m$, then MHAR $\ll$ RHMC.

Then, if $n^{1+\frac{1}{3}} \ll m$ we have an analytic guarantee that MHAR has a lower cost per sample than all of the other algorithms in Table 3. Moreover, empirical tests show that MHAR is faster than all of the other algorithms in Table 3 for regimes other than $n^{1+\frac{1}{3}} \ll m$.

6   MHAR Empirical Test

This section details a series of experiments to compare MHAR against the *hitandrun* library used by [Tervonen et al.(2013)Tervonen, Valkenhoef, Basturk, and Postmus]. We compare the running times in simplexes and hypercubes of different dimensions and for

25

⁴⁷³ various values of the padding hyper-parameter z. We also test the robustness of MHAR

⁴⁷⁴ by conducting empirical analyses similar to those in [Tervonen et al.(2013)Tervonen, Valkenhoef, Basturk

⁴⁷⁵ MHAR experiments were run in a Colab Notebook equipped with an Nvidia P100 GPU,

⁴⁷⁶ and a processor Intel® Xeon® CPU running at 2.00 GHz, and 14 GB of RAM. Due

⁴⁷⁷ to its apparent incompatibility with the Colab Notebook, the *hitandrun* experiments

⁴⁷⁸ were run in a <device> equipped with an Intel® Core™ i7-7700HQ CPU running at

⁴⁷⁹ 2.80 GHz and 32 GBs of RAM. All experiments used 64 bits of precision.

We formally define the n-simplex and the n-hypercube as

$$n\text{-simplex} = \{x \in \mathbb{R}^n \| \sum x_i = 1, x \geq 0\}, \tag{19}$$

$$n\text{-hypercube} = \{x \in \mathbb{R}^n \| x \in [-1, 1]^n\}. \tag{20}$$

⁴⁸⁰ ## 6.1   The Code

⁴⁸¹ The MHAR code was developed using python, and the Pytorch library was chosen

⁴⁸² because of its flexibility, power, and popularity [Paszke et al.(2019)]. Pytorch also

⁴⁸³ works in a CPU without need of a GPU, although the latter is more suitable for large

⁴⁸⁴ samples in high dimensions. The MHAR experiments were performed without observing

⁴⁸⁵ any numerical instabilities, and the maximum error found for the inversion matrix was

⁴⁸⁶ on the order $1e$-16, which is robust enough for most applications. Operations such

⁴⁸⁷ as matrix inversion, random number generation, matrix-to-matrix multiplication, and

⁴⁸⁸ point-wise operations were carried out in the GPU. The only operations that needed to

⁴⁸⁹ be carried out in the CPU were reading the constraints and saving the samples to disk.

⁴⁹⁰ For the rest of this section, the acronyms MHAR and HAR refer to the actual

⁴⁹¹ implementations and not the abstract algorithms. The code is available in `https:`

⁴⁹² `//github.com/uumami/mhar_pytorch`.

6.2   The padding

The padding hyper-parameter z determines the number of simultaneous walks the al-
gorithm performs. We generated 10 MHAR runs for each dimension (5, 25, 50, 100,
500, 1000) and each padding value (z) on simplexes and hypercubes. At each run we
calculated the average samples per second as follows:

$$Avg.\ Samples\ per\ Second = \frac{Total\ Samples}{Time} = \frac{z \times \varphi \times T}{Time}.$$

For example, z might equal 100, the thinning parameter φ might equal 30,000, and the
number of iterations T might equal 1, which would yield $3,000,000$ samples. If the
experiment took 1,000 seconds, the average samples per second would be $3,000$.
Figures 3 and 4 show box-plots for the experiments in dimensions 5 and 1000 for
the simplex and the hypercube, respectively. The box-plots for the the simplex and the
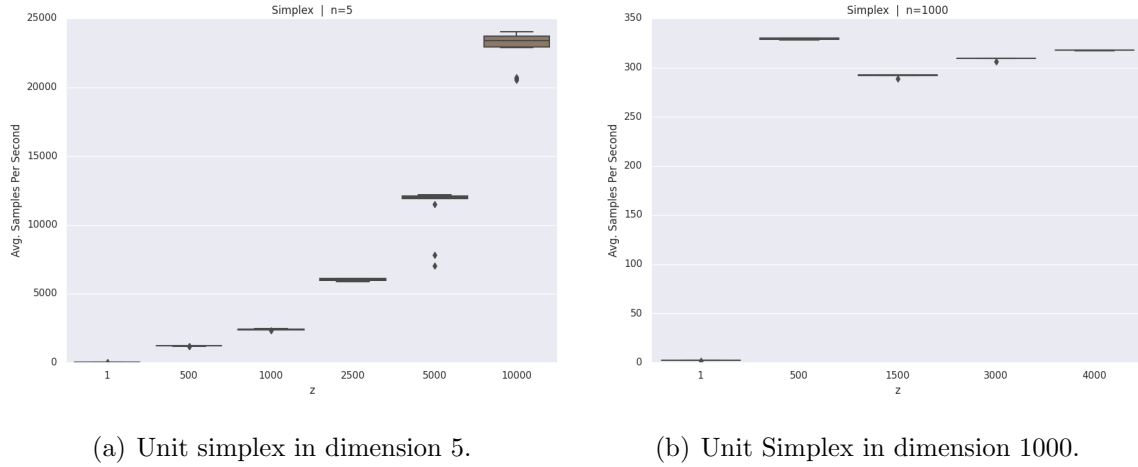hypercube in dimensions 25, 50, 100 and 500 can be found in Figures 6 and 7 in A.

(a) Unit simplex in dimension 5. (b) Unit Simplex in dimension 1000.

Figure 3: Box-plots for simplexes comparing padding behavior . In the y-axis the aver-
age samples per second are in thousands for different values of the padding parameter
z.

The box in the box-plots show the 25%, 50%, and 75% percentiles. The diamonds
mark outliers, and the upper and lower limits mark the maximum and minimum values
without considering outliers. For small values of z, larger padding yielded more average

samples per second. However, for some dimensions in the simplex and the hypercube, there was a value of z for which efficiency was lower. We conjecture that at some point large values of z could cause memory contention in the GPU.

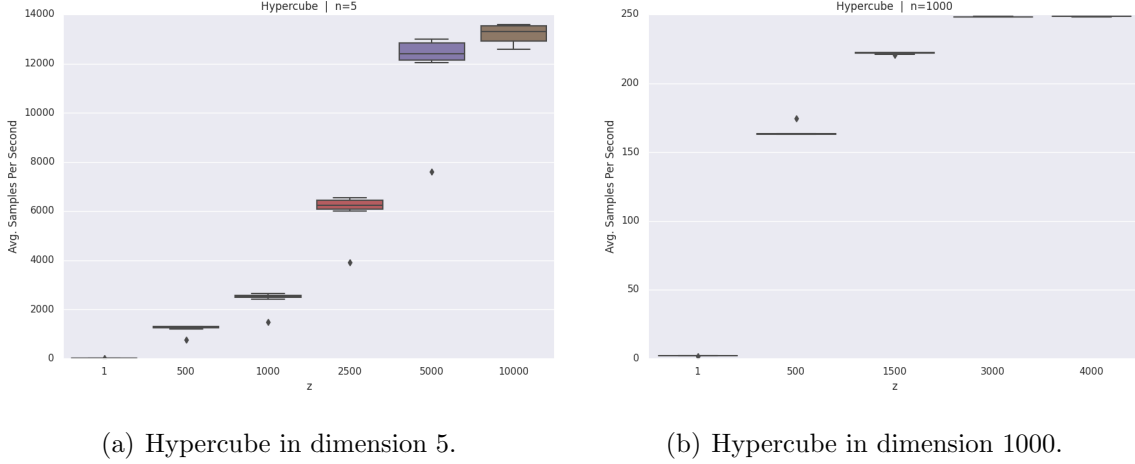(a) Hypercube in dimension 5. (b) Hypercube in dimension 1000.

Figure 4: Box-plots for hypercubes comparing padding behavior. In the y-axis the average samples per second are in thousands for different values of the padding parameter z.

6.3 Performance Test MHAR vs HAR

To compare MHAR and HAR we generated 10 simulations for different dimensions, and two types of polytopes (simplex and hypercubes). For the simplex we tested dimensions: 5, 25, 50, 100, and 250, and for the hypercube we tested dimensions: 5, 25, 50, 100, 500, and 1000. The *hitandrun* routines for sampling the simplex exhibited an extreme drop in performance at dimensions higher than 100 and memory contention at dimensions higher than 300.

For *hitandrun*, the total number of samples equals number of iterations times the thinning parameter. Because *hitandrun* does not make use of the GPU, the times are dependent on the CPU. Before running a given combination of convex body and dimension in MHAR, we selected the padding hyper-parameter z^* that had the highest average sampled points per second according to our padding experiments. So the z^*

⁵²² can differ by dimension. We used $\varphi = 30,000$ and $T = 1$. Table 4 summarizes the results.

Table 4: Performance of MHAR versus HAR for the optimal value of z^*

Figure	n	z	Performance ratio (MHAR mean / HAR mean)	Avg. Samples Per Second			
				MHAR mean	HAR mean	MHAR Std. Dev.	HAR Std. Dev.
Hypercube	5	10,000	14.18	13,206,089.93	931,368.92	376,068.96	57,727.69
Hypercube	25	5,000	29.05	10,839,474.35	373,127.77	1,236,619.81	77,786.96
Hypercube	50	2,500	21.85	5,151,516.81	235,742.22	612,241.73	20,636.30
Hypercube	100	4,000	116.77	4,363,525.70	37,367.93	10,619.65	1,486.54
Hypercube	500	4,000	95.21	621,554.24	6,528.56	782.70	157.76
Hypercube	1,000	4,000	248.32	248,513.69	1,000.79	182.97	18.15
Simplex	5	10,000	23.14	22,878,783.33	988,580.92	1,258,481.83	126,254.73
Simplex	25	10,000	1,343.58	24,338,761.06	18,114.90	168,300.75	409.27
Simplex	50	10,000	12,630.89	13,425,900.57	1,062.94	16,403.51	17.33
Simplex	100	3,000	128,348.67	7,255,837.08	56.53	135,616.62	0.88
Simplex	250	4,000	2,551,224.17	2,656,449.22	1.04	4,440.59	0.00

⁵²⁴ Table 4 shows substantial performance gains for MHAR. For the simplex, the gains
⁵²⁵ were greater at higher dimensions. The performance ratio (average samples per second
⁵²⁶ for MHAR divided by that for HAR) was 23 for $n = 5$ and 2.5 million for $n = 250$.
⁵²⁷ For the hypercube, performance gain for MHAR was also greater at higher dimensions.
⁵²⁸ Nevertheless, the performance ratio was 14 for $n = 5$ and 248 for $n = 1,000$.

⁵²⁹ In order to test the limits of our implementation, we conducted an additional set
⁵³⁰ of experiments for lower and higher dimensions and different padding parameters. We
⁵³¹ present these results in B.

⁵³² 6.4 Independence Test

⁵³³ To asses the convergence of MHAR to a uniform distribution, we conducted Friedman-
⁵³⁴ Rafsky two-sample Minimum Spanning Tree (MST) test [Friedman and Rafsky(1979)],
⁵³⁵ as was done in [Tervonen et al.(2013)Tervonen, Valkenhoef, Basturk, and Postmus]. The
⁵³⁶ test compares an obtained sample S (MHAR) with a sample U from the target distribu-
⁵³⁷ tion. The test defines an MST for S and U by counting the number of within- and across-
⁵³⁸ sample edges to assess if both samples come from the same distribution. The statistic
⁵³⁹ from the tests yields a *z-value* for the null hypothesis: "Both samples are drawn from the
⁵⁴⁰ same distribution." Authors in [Tervonen et al.(2013)Tervonen, Valkenhoef, Basturk, and Postmus]
⁵⁴¹ establish a threshold of $-1.64 \leq$ *z-value* to accept the null hypothesis.

29

A uniform sample U can quickly be drawn from the hypercube or the simplex
[Rubin(1981)] using known statistical methods. We generated 10 simulations in sim-
plexes and hypercubes in dimensions: 5, 15, 25, and 50, for a total of 80 simulations.
We used a single padding parameter (z) of 1000; and a "burning rate" (φ) of $(n-1)^3$ for
the simplex, and n^3 for the hypercube. Each simulation draw a total of 5000 samples
that were compared to an independently generated sample U each time.

Figure 5 shows the results from the experiments. The red dashed line represents
the threshold of $-1.64 \leq$ *z-value*. All simulations where above the expected threshold
with the exception of one single experiment for the simplex in dimension 25. This
experiments suggests that MHAR mixes fast from any starting point, supporting the
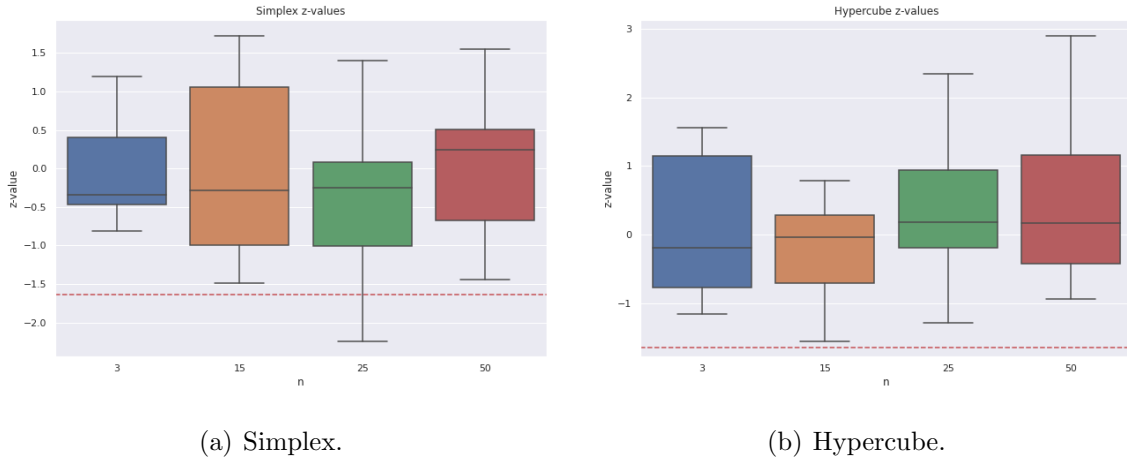uniform sample hypothesis.

(a) Simplex.   (b) Hypercube.

Figure 5: Friedman-Rafsky two-sample MST tests.

7   Conclusions

MHAR showed sustainable performance improvements over HAR while having a robust
uniform sampling. We hope that this technical advances move the scientific commu-
nity towards simulation approaches to complement the already established analytical
solutions. Our contribution was in creating the MHAR, analyzing its asymptotic be-

havior in terms of complexity and convergence, alongside a robust and easy to use implementation ready for deployment, including the cloud. Our implementation is substantially faster than existing libraries, especially for bigger dimensions. Additionally, we showed the versatility that Deep Learning frameworks, like Pytorch, can bring to support research.

We would like to emphasize the relevance of this work as a cornerstone to exploratory-optimization algorithms. The speedups we present in high dimensions makes it possible for many new practical applications to become a normal trend, expanding the range of solutions that engineering can provide. In particular, our previous work in Decision Analysis, Optimization, Game Theory, and Ambiguity Optimization will be significantly improved with this tool, and we think that many practitioners and researchers will be benefit as well.

Our implementation could be extended to multiple GPUs, possibly distributed. This will allow us to sample even larger polytopes using cloud architectures. Given the speed up results, a bounding approach for more general convex figures alongside accept-and-reject methods is worth exploring, especially for volume calculations.

Acknowledgments

References

[Chen et al.(2018)Chen, Dwivedi, Wainwright, and Yu] Y. Chen, R. Dwivedi, M. J. Wainwright, B. Yu, Fast mcmc sampling algorithms on polytopes, Journal of Machine Learning Research 19 (2018) 1–86.

[Lawrence(1991)] J. Lawrence, Polytope volume computation, Mathematics of Computation 57 (1991) 259–271.

[Lee and Vempala(2018)] Y. T. Lee, S. S. Vempala, Convergence rate of riemannian hamiltonian monte carlo and faster polytope volume computation, in: Proceedings of the 50th Annual ACM SIGACT Symposium on Theory of Computing, STOC 2018, Association for Computing Machinery, New York, NY, USA, 2018, pp. 1115–1121.

[Emiris and Fisikopoulos(2014)] I. Z. Emiris, V. Fisikopoulos, Efficient random-walk methods for approximating polytope volume, in: Proceedings of the Thirtieth Annual Symposium on Computational Geometry, Association for Computing Machinery, New York, NY, USA, 2014, pp. 318–327.

[Vempala and Bertsimas(2004)] S. Vempala, D. Bertsimas, Solving convex programs by random walks., Journal of the ACM 51 (2004) 540–556.

[Ma et al.(2019)Ma, Chen, Jin, Flammarion, and Jordan] Y. A. Ma, Y. Chen, C. Jin, N. Flammarion, M. I. Jordan, Sampling can be faster than optimization, Proceedings of the National Academy of Sciences 116 (2019) 20881–20885.

[Kannan and Narayanan(2013)] R. Kannan, H. Narayanan, Random walks on polytopes and an affine interior point method for linear programming, Mathematics of Operations Research 37 (2013) 1–20.

[Huang and Mehrotra(2015)] K. L. Huang, S. Mehrotra, An empirical evaluation of a walk-relax-round heuristic for mixed integer convex programs., Computational Optimization and Applications 60 (2015) 559–585.

[Feldman et al.(2005)Feldman, Wainwright, and Karger] J. Feldman, M. J. Wainwright, D. R. Karger, Using linear programming to decode binary linear codes., IEEE Transactions on Information Theory 51 (2005) 954–972.

[Kapfer and Krauth(2013)] S. Kapfer, C., W. Krauth, Sampling from a polytope and hard-disk monte carlo, Journal of Physics: Conference Series 454 (2013) 012031.

[Tervonen et al.(2013)Tervonen, Valkenhoef, Basturk, and Postmus] T. Tervonen, v. Valkenhoef, G., N. Basturk, D. Postmus, Hit-and-run enables efficient weight generation for simulation-based multiple criteria decision analysis, European Journal of Operational Research 224 (2013) 168–184.

[Montiel and Bickel(2013a)] L. V. Montiel, E. J. Bickel, Approximating joint probability distributions given partial information, Decision Analysis 10 (2013a) 26–41.

[Montiel and Bickel(2013b)] L. V. Montiel, E. J. Bickel, Generating a random collection of discrete joint probability distributions subject to partial information, Methodology and Computing in Applied Probability 15 (2013b) 951–967.

[Geyer and Charles(1992)] Geyer, J. Charles, Practical markov chain monte carlo, Statistical Science 7 (1992) 473–483.

[Gordon et al.(1993)Gordon, Salmond, and M.] N. J. Gordon, D. J. Salmond, S. A. F. M., Novel approach to nonlinear/non-gaussian bayesian state estimation., EE Proceedings F Radar and Signal Processing 140 (1993) 107–113.

[Montiel and Bickel(2012)] L. V. Montiel, E. J. Bickel, A simulation-based approach to decision making with partial information, Decision Analysis 9 (2012) 329–347.

[Montiel and Bickel(2014)] L. V. Montiel, E. J. Bickel, A generalized sampling approach for multilinear utility functions given partial preference information, Decision Analysis 11 (2014) 147–170.

[Cid and Montiel(2019)] G. M. Cid, L. V. Montiel, Negociaciones de máxima probabilidad para juegos cooperativos con fines comerciales, Revista mexicana de economía y finanzas 14 (2019) 245–259.

[Smith(1996)] R. L. Smith, The hit-and-run sampler: a globally reaching markov chain sampler for generating arbitrary multivariate distributions, Proceedings of the 1996 Winter Simulation Conference (1996).

[Lovász(1999)] L. Lovász, Hit-and-run mixes fast, Mathematical Programming 86 (1999) 443–461.

[Umans(2006)] C. Umans, Group-theoretic algorithms for matrix multiplication, Proceedings of the 2006 International Symposium on Symbolic and Algebraic Computation - ISSAC '06 (2006).

[Knight(1995)] P. A. Knight, Fast rectangular matrix multiplication and qr decomposition, Linear Algebra and Its Applications 221 (1995) 69–81.

[Li et al.(2011)Li, Ranka, and Sahni] J. Li, S. Ranka, S. Sahni, Strassen's matrix multiplication on gpus, in: 2011 IEEE 17th International Conference on Parallel and Distributed Systems, 2011, pp. 157–164.

[Press et al.(2007)Press, Teukolsky, Vetterling, and Flannery] W. H. Press, S. A. Teukolsky, W. T. Vetterling, B. P. Flannery, Numerical Recipes 3rd Edition: The Art of Scientific Computing, 3rd ed., Cambridge University Press, 2007.

[Huang et al.(1993)Huang, Yu, and van de Geijn] J. Huang, C. D. Yu, R. A. van de Geijn, Implementing Strassen's Algorithm with CUTLASS on NVIDIA Volta GPUs, Technical Report, The University of Texas at Austin, 1993.

[Lee and Vempala(2017)] Y. T. Lee, S. S. Vempala, Geodesic walks in polytopes, in: Proceedings of the 49th Annual ACM SIGACT Symposium on Theory of Computing, STOC 2017, Association for Computing Machinery, New York, NY, USA, 2017.

[Lovász and Simonovits(1993)] L. Lovász, M. Simonovits, Random walks in a convex body and an improved volume algorithm, Random Structures and Algorithms 4 (1993) 359–412. arXiv:https://onlinelibrary.wiley.com/doi/pdf/10.1002/rsa.3240040402.

[Cormen et al.(2009)Cormen, Leiserson, Rivest, and Stein] T. H. Cormen, C. Leiserson, R. Rivest, C. Stein, Introduction to Algorithms, 3rd ed., MIT Press, 2009.

[Lovász and Vempala(2006)] L. Lovász, S. Vempala, Hit-and-run from a corner, SIAM Journal on Computing 35 (2006) 985–1005.

[Vaidya(1989)] P. M. Vaidya, Optimization by simulated annealing, 30th Annual Symposium on Foundations of Computer Science (1989).

[Marsaglia(1972)] G. Marsaglia, Choosing a point from the surface of a sphere., The Annals of Mathematical Statistics 43 (1972) 645–646.

[Chay et al.(1975)Chay, Fardo, and Mazumdar] S. C. Chay, R. D. Fardo, M. Mazumdar, On using the box-muller transformation with multiplicative congruential pseudo-random number generators, Journal of the Royal Statistical Society. Series C (Applied Statistics) 24 (1975) 132–135.

[Gustafson and Narayanan(2018)] A. Gustafson, H. Narayanan, John's walk, 2018. arXiv:1803.02032.

[Paszke et al.(2019)] A. Paszke, et al., Pytorch: An imperative style, high-performance deep learning library, in: Advances in Neural Information Processing Systems 32, Curran Associates, Inc., 2019, pp. 8026–8037.

[Friedman and Rafsky(1979)] J. H. Friedman, L. C. Rafsky, Multivariate generalizations of the wald-wolfowitz and smirnov two-sample tests, The Annals of Statistics 7 (1979) 697–717.

[Rubin(1981)] D. B. Rubin, The bayesian bootstrap, The Annals of Statistics 6 (1981) 130–134.

A Additional Optimal Padding Experiments

Here we present the results for different padding parameters using 10 MHAR runs for each dimension (25, 50, 100, 500) on simplexes and hypercubes. Figure 6 shows the box-plots for simplexes while Figure 7 shows the box-plots for hypercubes.

(a) Unit simplex in dimension 25.

(b) Unit simplex in dimension 50.

(c) Unit simplex in dimension 100.
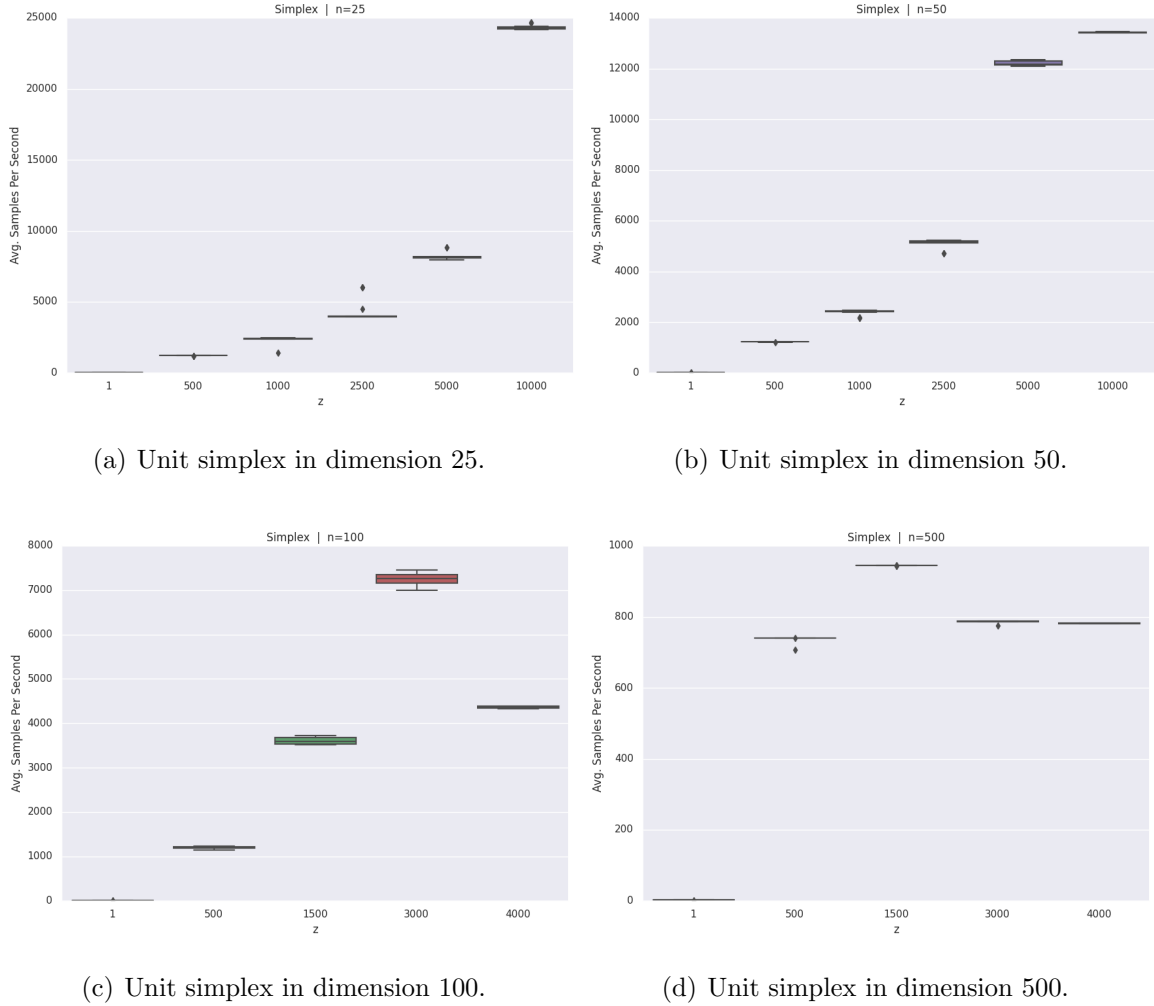
(d) Unit simplex in dimension 500.

Figure 6: Box-plots for simplexes comparing padding behavior. In the y-axis the average samples per second are in thousands for different values of the padding parameter z.

The box in the boxplots show the 25%, 50%, and 75% percentiles. The diamonds mark outliers, and the upper and lower limits mark the maximum and minimum values without considering outliers.

35

(a) Hypercube in dimension 25.

(b) Hypercube in dimension 50.

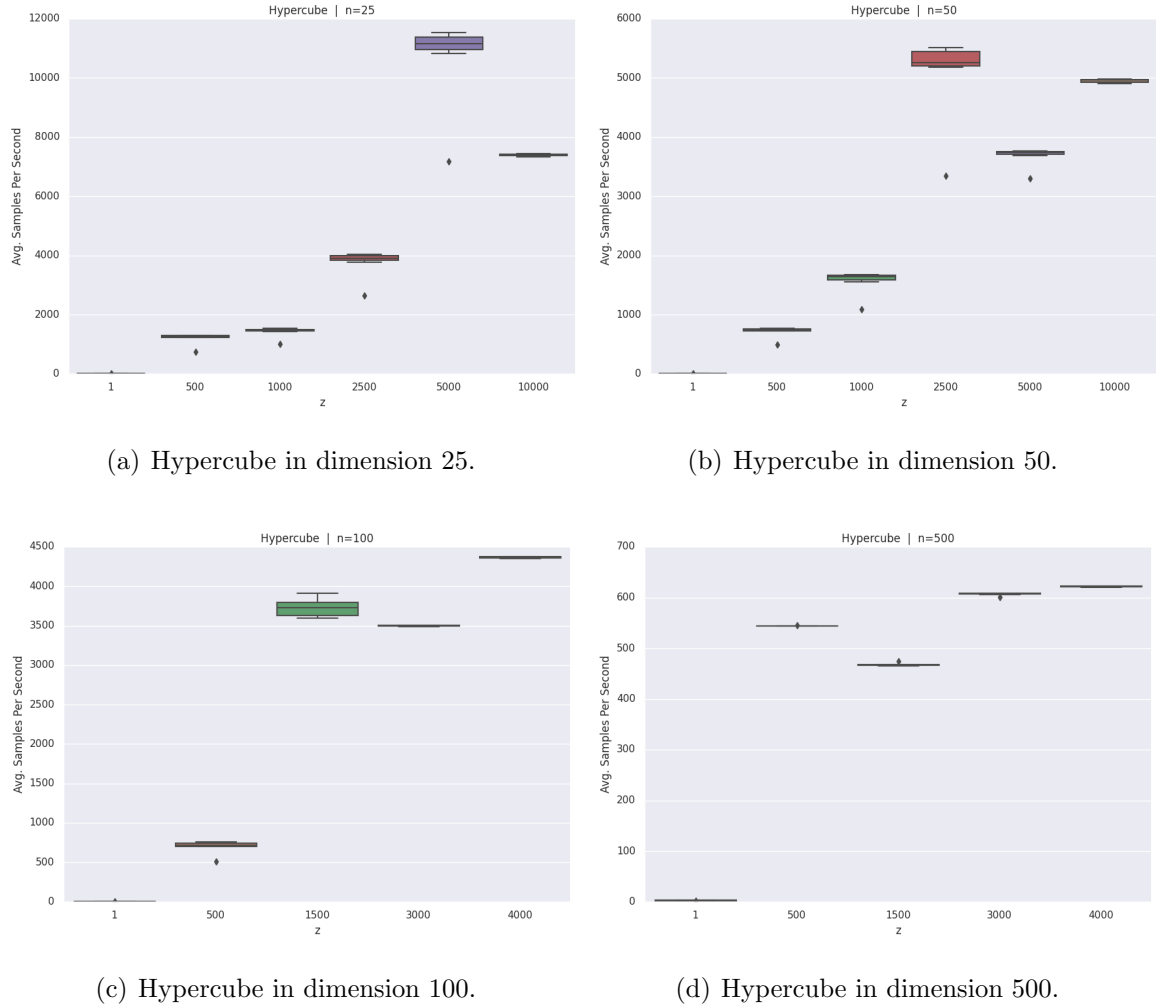(c) Hypercube in dimension 100.

(d) Hypercube in dimension 500.

Figure 7: Box-plots for hypercube comparing padding behavior. In the y-axis the average samples per second are in thousands for different values of the padding parameter z.

B   Additional Performance Experiments

Here we present some additional experiments of the fitness of the MHAR. Table 5 reports the running times and the average sampled points per second for the best values of z for each combination of figure and dimension. For each combination, we conducted the experiment 10 times. Table 5 shows that average samples per second is lower for higher dimensions, due to the curse of dimensionality. However, the performance of MHAR is outstanding.

36

Table 5: Samples Per Second of the MHAR.

				Avg. Samples Per Second		Running Time (seconds)	
Figure	n	z	Total Samples	Mean	Std. Dev.	Mean	Std. Dev.
Hypercube	3	10,000	300,000,000	25,357,073.87	675,444.40	11.84	0.32
Hypercube	5	10,000	300,000,000	13,206,089.93	376,068.96	22.73	0.66
Hypercube	15	10,000	300,000,000	25,344,794.68	655,021.48	11.84	0.31
Hypercube	25	5,000	150,000,000	10,839,474.35	1,236,619.81	14.07	2.28
Hypercube	50	2,500	75,000,000	5,151,516.81	612,241.73	14.83	2.54
Hypercube	100	4,000	120,000,000	4,363,525.70	10,619.65	27.50	0.07
Hypercube	250	3,000	90,000,000	1,219,419.53	8,630.27	73.81	0.53
Hypercube	500	4,000	120,000,000	621,554.24	782.70	193.06	0.24
Hypercube	1,000	4,000	120,000,000	248,513.69	182.97	482.87	0.36
Hypercube	2,500	1,500	15,000,000	50,808.74	15.02	295.22	0.09
Hypercube	5,000	1,000	10,000,000	16,161.69	5.92	618.75	0.23
Simplex	3	10,000	300,000,000	19,795,014.21	2,628,558.29	15.38	1.81
Simplex	5	10,000	300,000,000	22,878,783.33	1,258,481.83	13.15	0.77
Simplex	15	10,000	300,000,000	24,269,548.32	302,854.48	12.36	0.16
Simplex	25	10,000	300,000,000	24,338,761.06	168,300.75	12.33	0.08
Simplex	50	10,000	300,000,000	13,425,900.57	16,403.51	22.34	0.03
Simplex	100	3,000	90,000,000	7,255,837.08	135,616.62	12.41	0.23
Simplex	250	4,000	120,000,000	2,656,449.22	4,440.59	45.17	0.08
Simplex	500	1,500	45,000,000	944,784.52	583.24	47.63	0.03
Simplex	1,000	500	15,000,000	329,315.49	556.62	45.55	0.08
Simplex	2,500	500	5,000,000	77,312.01	3,045.62	64.78	2.86
Simplex	5,000	1,000	10,000,000	22,437.63	62.27	445.68	1.25

Note: The table contains the performance statistics obtained during the MHAR experiments for the best possible value of z we could find.